Separating Structural Heterogeneities from Stochastic Variations in Fluorescence Resonance Energy Transfer Distributions via Photon Distribution Analysis

Matthew Antonik,* Suren Felekyan, Alexander Gaiduk, and Claus A. M. Seidel*

Institut für Physikalische Chemie, Lehrstuhl für Molekulare Physikalische Chemie, Heinrich-Heine-Universität, Universitätsstraβe 1, Geb 26.32, 40225 Düsseldorf, Germany

Received: December 12, 2005; In Final Form: February 2, 2006

We establish a probability distribution analysis (PDA) method for the analysis of fluorescence resonance energy transfer (FRET) signals to determine with high precision the originating value of a shot-noise-limited signal distribution. PDA theoretical distributions are calculated explicitly including crosstalk, stochastic variations, and background and represent the minimum width that a FRET distribution must have. In this way an unambiguous distinction is made between shot-noise distributions and distributions broadened by heterogeneities. This method simultaneously and effectively extracts highly resolved information from FRET distributions. The theoretical histograms match the exact profile of histograms generated from constant transfer efficiency experimental data with a χ^2 near unity. The χ^2 surface suggests an ultimate level of precision with FRET of <1% of the Förster radius. Distributions of FRET signals in donor−acceptor-labeled DNA were unambiguously identified as being broader than shot-noise variations could explain. A model describing a Gaussian distribution of distances was tested with the PDA method and demonstrated 5 Å inhomogeneities due to dye motions. The capability of this method to recover quantitative information from FRET distributions has potential applications for studying molecular conformations and dynamics. Potential sources for artifacts such as acceptor photobleaching, spectrally different observation volumes, and fluctuations of the Förster radius are ruled out.

1. Introduction

Conformational changes and fluctuations in molecular interactions are essential for many chemical reactions and biological processes. Distributions of fluctuations provide valuable information about the topography of the molecular energy landscape and are critical to understanding chemical dynamics, protein folding, conformational activity, and noncovalent binding.[1−4] Confocal fluorescence techniques have gained considerable interest in investigating molecular fluctuations because they do not perturb the system and can be carried out in solution at physiological conditions. Moreover, at the single-molecule level they can examine dynamic behavior directly without ensemble averaging.[5,6] Fluorescence resonance energy transfer (FRET) is a technique in which a single molecule or complex is labeled with two dyes and the efficiency of energy transfer from one dye to the other is monitored. The transfer efficiency, and hence the fluorescence intensities of both dyes, is sensitive to their relative positions, orientations, and fluorescence properties.[7] As such, signal distributions reflect conformational activity and changes in the local environment.[6] Analysis of FRET signal distributions has revealed folding pathways, intermediates, and conformational activity in proteins,[8−11] RNA,[12] and DNA.[13]

A central difficulty in extracting molecular information from fluorescence intensity distributions has been the inability to unambiguously distinguish molecular fluctuations from either stochastic variations or background counts, especially when signal counts are low.[14;15] We establish here a probability distribution analysis (PDA) method that quantitatively and precisely describes the shapes of FRET signal distributions measured by two-color photon-counting techniques. By inclusion of the effects of background and stochastic processes, the shot-noise-limited shapes of histograms generated from single-photon-counting data can be predicted with high precision.

2. Theory

2.1. Fluorescence Signals. In FRET, a donor molecule, D, is excited and the energy can be nonradiatively transferred to an acceptor molecule, A. The efficiency of energy transfer, E, is determined by the proximity and orientations of D and A, the spectral overlap between donor emission and acceptor excitation, and the quantum yields of the molecules. E is usually interpreted as the fraction of energy that was transferred to the acceptor during a measurement, but in our case it will be viewed as the probability that the energy from any given photon absorbed by the donor is transferred to the acceptor.

The amount of energy transfer in FRET experiments can be measured by separating signal photons into two spectral regions corresponding to the donor and the acceptor emission spectra. Green and red spectral regions are used here, denoted by the subscripts G and R, respectively. A distinction between donor/acceptor and green/red must be made because the terms donor/acceptor refer exclusively to photons that originate via fluorescence at the molecules, whereas the terms green/red are descriptive terms indicating in which channel events are counted and can equally be applied to either fluorescence, scatter, crosstalk, or nonphoton dark counts. Thus, the measured signal is a number of counts in the red and green channels, S_G and S_R, consisting of a number of fluorescence photons arriving at the green/red detectors, F_G and F_{RT}, and a number of background

* Authors to whom correspondence should be addressed. Phone: +49 (211) 811 5881. Fax: +49 (211) 811 2803. E-mail: matthew.antonik@uni-duesseldorf.de; cseidel@gwdg.de.

10.1021/jp057257+ CCC: $33.50
Published on Web 03/15/2006

counts, B_G and B_R. The subscript in F_{RT} represents the total fluorescence signal appearing in the red channel, including counts that were emitted by the donor but detected in the red channel (crosstalk). The total number of events counted is given by $N = F_G + F_{RT} + B_G + B_R$.

2.2. Probability Distribution Analysis. The PDA method calculates the theoretical probability of recording a particular combination of F_G, F_{RT}, B_G, and B_R, from which any intensity-based parameter, such as proximity ratio or FRET efficiency, can be derived. The signal ratio, $S_G/S_R = (F_G + B_G)/(F_{RT} + B_R)$, is chosen as the parameter of interest here because the predicted distributions can be compared directly to the uncorrected, unmodified experimental data. Since photon counting results in a finite set of ratio values, the particular values will be denoted by $(S_G/S_R)_i$, and the probability of observing that value by $P(S_G/S_R)_i$. Many $(S_G/S_R)_i$ values can be obtained from several different combinations of F_G, F_{RT}, B_G, and B_R, so $P(S_G/S_R)_i$ is calculated by summing the probability of each combination

$$P\left(\frac{S_G}{S_R}\right)_i = \sum_{\substack{\text{all } F_G,F_{RT},B_G,B_R \\ \text{which yield } (S_G/S_R)_i}} P(F_G,F_{RT},B_G,B_R) \quad (1)$$

Equation 1 can be factored into a product of independent probabilities. B_G and B_R are independent of each other and of the number of fluorescence photons and so are written as separate factors, $P(B_G)$ and $P(B_R)$. The remaining term, $P(F_G,F_{RT})$, describes the probability of observing a particular combination of green and red photons. This term is equivalent to the probability of observing a total of $F = F_G + F_{RT}$ fluorescence photons times the probability that exactly F_{RT} out of F photons are red; $P(F_G,F_{RT}) = P(F) \times P(F_{RT}|F)$. Making these changes to eq 1 results in

$$P\left(\frac{S_G}{S_R}\right)_i = \sum_{\substack{\text{all } F,F_{RT},B_G,B_R \\ \text{which yield } (S_G/S_R)_i}} P(F)P(F_{RT}|F)P(B_G)P(B_R) \quad (2)$$

The latter three terms in eq 2 can be described analytically. First, under the restriction that the data are measured in equal time windows, the probability of recording B_G and B_R background photons per time window, $P(B_G)$ and $P(B_R)$, assuming average counts per time window values of $\langle B_G\rangle$ and $\langle B_R\rangle$ respectively, is given by the Poisson distribution as shown in eq 3.[16] Second, assuming there is a fixed probability, ϵ, that any given count is recorded in the red channel, the probability of observing exactly F_{RT} red fluorescence photons out of F total fluorescence photons can be expressed as a binomial distribution. $P(F_{RT}|F)$ is written from here on with a subscript ϵ in eq 4 to indicate this assumption

$$P_{\langle B\rangle}(B) = \frac{\langle B\rangle^B e^{-\langle B\rangle}}{B!} \quad (3)$$

$$P_\epsilon(F_{RT}|F) = \frac{F!}{F_{RT}!(F-F_{RT})!}\epsilon^{F_{RT}}(1-\epsilon)^{F-F_{RT}} \quad (4)$$

The parameter ϵ is an apparent FRET efficiency, which differs from E according to the quantum yields, detection efficiencies, and crosstalk of the system. A quantitative description of ϵ is provided below.

The final term that needs to be considered in eq 2 is the fluorescence intensity distribution $P(F)$. Analytical descriptions have been described in the literature,[16] but it would be simpler to substitute a measurable quantity for $P(F)$. Any particular term in eq 2 is evaluated only after B_G and B_R are specified. This fact suggests that the fluorescence intensity can be calculated as $F = N - B_G - B_R$. Making this substitution, changing the sum to occur over all values for N and replacing $P(F)$ with $P(N)$ leads to eq 5

$$P\left(\frac{S_G}{S_R}\right)_i = \sum_{\substack{\text{all } N,F_{RT},B_G,B_R \\ \text{which yield } (S_G/S_R)_i}} P(N)P_\epsilon(F_{RT}|N-B_G-B_R) \times P_{\langle B_G\rangle}(B_G)P_{\langle B_R\rangle}(B_R) \quad (5)$$

The distributions $P_{\langle B_G\rangle}$, $P_{\langle B_R\rangle}$, and P_ϵ are given by eqs 3 and 4. To obtain $P(N)$, the total intensity distribution histogram can be normalized. $\langle B_G\rangle$ and $\langle B_R\rangle$ are calculated from the mean background count rates. Only ϵ remains unknown and may be determined by using a χ^2 maximum likelihood estimator fit.

2.3. Apparent Transfer Efficiency ϵ. The conventional FRET efficiency describes the ratio of sensitized acceptor events to the total number of donor excitations. If the intensity of fluorescence emissions from D and A are known (F_D and F_A, respectively), then E can be calculated according to eq 6

$$E = \frac{F_A/\Phi_{FA}}{F_D/\Phi_{FD} + F_A/\Phi_{FA}} \quad (6)$$

Φ_{FD} and Φ_{FA} are the fluorescence quantum yields of the donor and the acceptor, respectively. In practice, not all fluorescence emissions are detected. F_G and F_{RT} differ from F_D and F_A by the detection efficiency factors g_G and g_R, respectively. Additionally, the overlap of the donor and the acceptor fluorescence spectra results in a fraction of the donor signal appearing in the red channel, characterized by a spectral crosstalk term, α, which appears in eq 7 (for definitions, see section 3.2)

$$F_G = g_G F_D$$
$$F_{RT} = g_R F_A + \alpha g_G F_D \quad (7)$$

Combining eqs 6 and 7, the apparent efficiency can be defined as a function of more conventional fluorescence parameters

$$\epsilon = \frac{F_{RT}}{F_G + F_{RT}} = 1 - \frac{1}{1 + \frac{\Phi_{FA}g_R}{\Phi_{FD}g_G}\frac{E}{(1-E)} + \alpha} \quad (8)$$

2.4. Experimental Considerations. Equations 3, 4, 5, and 8 provide an analytical expression for the probability of any particular value of $(S_G/S_R)_i$ given $P(N)$, $\langle B_G\rangle$, $\langle B_R\rangle$, and ϵ. Although ϵ is a natural parameter in terms of mathematical development, it is not used in the literature. Therefore, instead of ϵ in subsequent analysis, the more conventional fluorescence ratio, F_G/F_R, will be used. To emphasize the distinction between an observed ratio that varies stochastically and the characteristic ratio that defines the distribution, the term "originating value" is introduced and is denoted by brackets: $\langle F_G/F_R\rangle = [\epsilon/(1-\epsilon) - \alpha]^{-1}$. F_R is distinguished from F_{RT} by excluding crosstalk photons, $F_R = F_{RT} - \alpha g_G F_D$, a convention that conforms to previously published reports.[17]

Histograms are generated from $P(S_G/S_R)$ distributions by allocating each $(S_G/S_R)_i$ to a specific bin, summing all $P(S_G/S_R)_i$ values that fall in the same bin and multiplying by the total number of molecules (or time windows) to be considered. It should be noted here that Poisson distributions have no upper bound, meaning it is possible to have more background photons than total photons. Consequently, for each value of N the Poisson distribution is calculated only up to N total counts, and the sum is subsequently normalized to unity.

3. Materials and Methods

3.1. Chemicals. For the single-dye experiments, an ultrapure sample of Atto590 (Atto-Tec, Siegen, Germany) was obtained from the company and diluted into deionized water at a pH of 6. For the FRET experiments, fluorescently labeled double-stranded 27-mer DNA was used, which has been previously described.[18] Alexa488 (donor, Molecular Probes) and Cy5 (acceptor, Amersham-Pharmacia) were used as the FRET pair, offering a large Förster radius of $R_0 = 51$ Å and well-separated emission wavelengths between the dyes. The quantum yields of the donor and acceptor are $\Phi_{FD} = 0.80$ and $\Phi_{FA} = 0.32$, respectively. Φ_{FA} already includes a factor of 0.8 that accounts for the fraction of time the acceptor is in the fluorescent trans conformation.[18] The DNA strands were synthesized by the standard aminophosphoramidite technology. In the (+)-strands, Cy5 was attached at a fixed site at the 5′-end via a C6-linker and a 5′-amino modifier (C6). Unlabeled complementary DNA (−)-strands were produced for use in the donor-only experiments as well as (−)-strands with Alexa488, attached via a C6-linker, to a thymidine residue 13 bp from the end, designated here as the DA-13 DNA (Amino-Modifier C6 dT from Glenresearch). The FRET efficiency for the donor−acceptor-labeled system was previously determined to be 0.4.[18] In all experiments, we used a sodium phosphate buffer with 180 mM NaCl, 10 mM NaH_2PO_4/Na_2HPO_4, and 400 μM Na−ascorbate (pH 7.5).

3.2. Fluorescence Detection. The experiments were performed using the same multiparameter fluorescence detection (MFD) techniques used for biological samples.[9] Single-molecule fluorescence detection was performed using a confocal epi-illuminated microscope with excitation by either a continuous-wave He−Ne laser at 594 nm for the Atto590 experiments or an active mode-locked Ar^+ laser (73.5 MHz, 150 ps) (Inova Sabre, Coherent, Palo Alto, CA) at 496.5 nm for the DNA experiments. The linearly polarized beam is focused into solution with a 60× 1.2 water-immersion objective (UPlan Apo, Olympus, Hamburg, Germany). The diameter of the focus was estimated to be $2\omega_{0E} = 1.17$ μm in the xy-plane based on the diffusion time of free Rh110 in water ($t_D = 0.293$ ms) as measured by fluorescence correlation spectroscopy (FCS). The parameter ω_{0E} is the radial distance from the optical axis of the excitation beam to where the intensity has dropped by a factor of e^2. The laser power at the objective was 439.2 μW, corresponding to a mean irradiance of $I_0/2 = 42.7$ kW/cm^2 in this focus. Fluorescence detection is performed with the same objective but with a confocal pinhole ($\varnothing = 100$ μm) that results in a detection volume of ~2 fL. The observation focus diameter in the xy-plane, $2\omega_{0O} = 1.6$ μm, is defined by the size of the pinhole and the magnification of the objective lens.

Sample molecules diffusing freely through the solution occasionally pass through the detection volume, resulting in a brief (~3 ms) burst of fluorescence. Dilute solutions of molecules (~50 pM) ensure that only single molecules are detected, with each burst corresponding to a single molecule. The fluorescence signal is separated from the laser light by a dichroic beam splitter (502/636 PC AHF Analyzentechnik, Tübingen, Germany) and further divided into parallel and perpendicular components and separated by a dichroic beam splitter (Q595LPXR, AHF Analyzentechnik, Tübingen, Germany) into wavelength ranges below and above 595 nm for the DNA experiments (green and red, respectively; filters, HQ535/50, HQ730/140 AHF Analyzentechnik, Tübingen, Germany) and below and above 655 nm for the Atto590 experiments (dichroic, DCSBXR 655; filters, HQ630/60, HQ680/60). The photons are detected by four avalanche photodiodes (APD) (SPCM AQR-14, EG&G Vandreuil, Quebec, Canada) coupled to a PC-based time-correlated single-photon-counting (TCSPC) module (SPC 432 or modified SPC 132, Becker and Hickel GmbH, Berlin, Germany) or a correlator board with a time resolution of 12.5 ns (ALV5000 with fast option, ALV GmbH, Langen, Germany). The signals S_G and S_R consist of counts, for each of which several parameters are recorded. The time since the last count and the detector number, corresponding to the polarization and color channel, are in all cases recorded in the TCSPC data. In addition, the arrival time after the laser pulse is recorded for the pulsed excitation DNA measurements.

The mean background count rates $\overline{B_G}$ and $\overline{B_R}$ (in kHz) are measured in a clean buffer solution. The spectral crosstalk coefficient is determined from the average signal count rates of a measurement of donor dye in buffer as $\alpha = (\overline{S_R} - \overline{B_R})/(\overline{S_G} - \overline{B_G})$. The notations $\overline{S_G}$, $\overline{S_R}$, $\overline{B_G}$, and $\overline{B_R}$ refer to average count rates, whereas the signals S_G, S_R, B_G, and B_R refer only to an integer number of counts in a specified time window. The detection efficiencies were calculated from the transmission function of the optics, $g'(\lambda)$, and the normalized fluorescence spectrum of the dye, $f(\lambda)$, according to $g = \int g'_{optics}(\lambda) \times f_{dye}(\lambda)\, d\lambda$.

3.3. PDA FRET Analysis. Single-molecule events were distinguished from the 3−6 kHz background by an intensity threshold criterion.[19] For Atto590, the single-molecule bursts were further subdivided into 1 ms time windows, and S_G/S_R was calculated directly.

Due to bleaching, incomplete labeling, and multiple donor species, the bursts obtained from DNA measurements required two selection steps before analysis. For step 1, bleaching correction, bursts in which a dye bleaches are identified by their nonoverlapping green and red signals. Averaging the macro time (laboratory time) of all green photons in a burst should produce the same average time T_G as the average macro time of all red photons T_R. In the case of a bleaching event, one dye will fluoresce longer than the other, which will result in different mean macro times. A threshold criterion of ±0.5 ms for the difference of mean green and red macro times $T_G - T_R$ was used to identify bleached molecules. This step typically reduced the amount of the high FRET ratio signal ($S_G/S_R > 4$) from 27% to 22% of the total signal [20] For step 2, selection of an individual donor population, plotting the signal ratio versus donor fluorescence lifetime in the presence of the acceptor, S_G/S_R vs $\tau_{D(A)}$, for the selected bursts revealed the effects of incomplete labeling and multiple donor lifetimes. According to criteria described in the text for each subensemble, only molecules are selected for further analysis that correspond to properly labeled, nonbleached molecules of a single population. These single-molecule bursts were further subdivided into 1 ms time windows, and S_G/S_R was calculated.

For each data set, a histogram of S_G/S_R was generated. The buffer for the DNA experiment contained a minor contamination species that accounted for ~0.6% of the bursts, for which the DNA histograms were corrected.[21] For calculation of the PDA

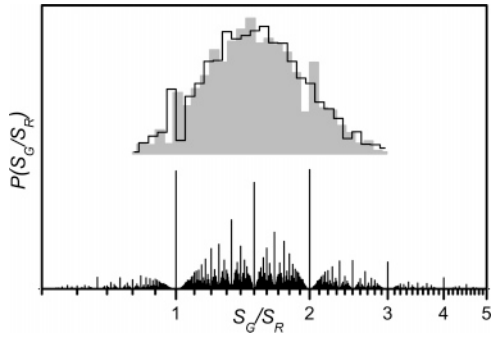

Figure 1. (Bottom) Comb plot indicating the probability of observing the possible S_G/S_R values. (Top) Two histograms composed from the comb plot probabilities, calculated from 0.5 to 5, with 49 bins (solid gray) and 50 bins (black line), showing the change in profile as the number of bins changes.

distributions, $P(N)$ intensity distributions are derived from the selected data from each experiment by making a histogram of the total number of photons per window, $N = S_G + S_R$, and dividing the histogram by the total number of time windows. $\langle B_G \rangle$ and $\langle B_R \rangle$ are calculated from $\overline{B_G}$ and $\overline{B_R}$, respectively, by multiplying by the duration of the time window (1 ms). A minimum threshold of $N \geq 20$ photons was set for the DNA analysis primarily to guarantee enough photons for a lifetime analysis and second to avoid donor-only artifacts. The threshold was applied to the Atto590 experiments for consistency with the DNA experiments. The goodness of fit between the data and the PDA histograms was determined using a χ^2 maximum likelihood test. A Levenberg−Marquadt optimization scheme was used to find the $\langle F_G/F_R \rangle$ that produced the minimum χ^2. Error bars were established by determining the values of $\langle F_G/F_R \rangle$ for which χ^2 was one higher than the minimum: $\chi^2 = \chi^2_{min} + 1$. Weighted residuals were calculated as (data histogram − PDA histogram)/$N_{bin}^{1/2}$, where N_{bin} is the number of data counts in the respective bins.

4. Results

4.1. PDA Distributions. To demonstrate several properties of the PDA distributions, eq 5 was evaluated for the arbitrary case of $N = 10-100$ photons, $\langle F_G/F_R \rangle = 1.5$, $\langle B_G \rangle = \langle B_R \rangle = 0$, and $\alpha = 0$. The $P(N)$ was taken from the DNA FRET data presented below. All of the probabilities between 0.5 and 5 are displayed without binning as a comb plot in Figure 1. The discrete nature of the distribution leads to two features that introduce binning artifacts in the generation of histograms: probability "spikes" at certain values and probability "voids" around the spikes.

Probability spikes are the result of the redundancy of certain values of the observed signal ratio. As a simple example, consider the case above, but with only $N = 1-10$ photons, and each N is equally likely. A value of $S_G/S_R = 1.5$ occurs twice in this set, 3/2 at $N = 5$ (3.45% chance) and 6/4 at $N = 10$ (6.27% chance). An $S_G/S_R = 1$ occurs 5 times, i.e., for every even N, with probabilities 4.80%, 3.45%, 2.76%, 2.32%, and 2.00%. Given the initial assignment of $\langle F_G/F_R \rangle = 1.5$, it is not surprising that the single most likely event is $S_G/S_R = 1.5$ at $N = 10$. However, when summed over all N, the value $P(S_G/S_R = 1.5) = 9.72\%$, which is lower than the 15.33% chance of observing $S_G/S_R = 1$. In essence, quantity wins over quality. The probability voids are observed because efficiency values near the spikes cannot be generated using only integer values between 10 and 100 inclusive.

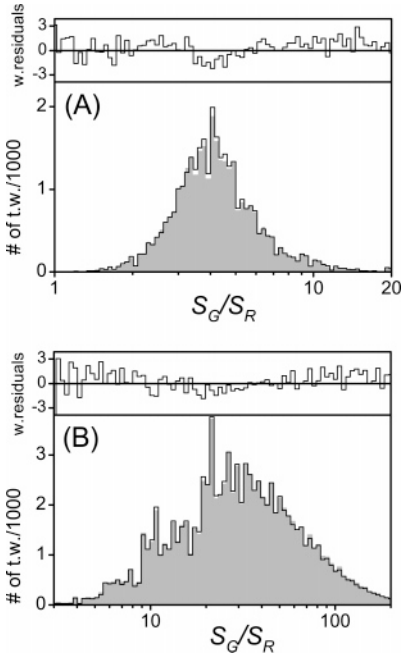

Figure 2. Histograms of the number of time windows with particular S_G/S_R values calculated from the data (gray areas) and predicted from the PDA method (black line) along with the weighted residuals for best PDA fits (above). (A) Atto590, $\langle F_G/F_R \rangle = 4.02$, $\langle B_G \rangle = 3.25$ counts, $\langle B_R \rangle = 0.76$ counts, $\alpha = 0$, and $\chi^2 = 1.30$. (B) donor-only-labeled DNA. $\langle F_G/F_R \rangle = \infty$, $\langle B_G \rangle = 3.83$ counts, $\langle B_R \rangle = 1.15$ counts, $\alpha = 0.01$, and $\chi^2 = 1.36$. $N = 20-444$ photons in both cases.

4.2. Single Dye: Fixed Efficiency. The investigation of the dye Atto590 was designed to simulate a FRET signal with a constant $\langle F_G/F_R \rangle$. Through the use of a single dye for both the green and the red signals, typical problems in FRET measurements such as variations in lifetime, anisotropy, quantum yield, and donor−acceptor distance are excluded. From eq 7, the red fluorescence signal consists of two terms corresponding to the two different dyes: an acceptor fluorescence term and a donor crosstalk term. Since there is only one dye in this experiment, only one term is necessary to describe F_{RT}, so the signal can be freely defined as either pure crosstalk ($g_R = 0$) or pure red fluorescence ($\alpha = 0$). Through the use of the latter definition and with recognition that $F_D = F_A$ and $\Phi_{FD} = \Phi_{FA}$, the expected signal ratio becomes $\langle F_G/F_R \rangle = g_G/g_R$. Assuming the instrumental properties remain constant, the signal ratio is sensitive only to shifts in the emission spectrum.

The resulting signal ratio histogram is shown in Figure 2A (bottom, solid gray histogram). Also shown in Figure 2A is the best-fit PDA histogram computed from eq 5 (solid line). It is clear that the theory predicts the shape of the histogram very well, including the positions and the heights of the individual spikes. The best fit, which shows no systematic deviations (Figure 2A, top), was determined to have a value of $\langle F_G/F_R \rangle = 4.02$. This is in agreement with the $\langle F_G/F_R \rangle = 3.65 \pm 0.56$ calculated from steady-state dye measurements and the manufacturer's specifications for the APDs.

4.3. DNA Donor Only. To confirm the homogeneous behavior of a single dye attached to DNA, donor-only-labeled DNA was investigated. Here, the crosstalk of $\alpha = 0.01$ is the only source of red fluorescence photons. An MFD analysis was performed on many single-molecule bursts. A look at the obtained S_G/S_R vs $\tau_{D(A)}$ histogram in Figure 3A shows that Alexa488 exists as two species: a long lifetime species with $\tau = 4$ ns (D1) and a minority lifetime species at $\tau = 2$ ns (D2). Although the two species have the same S_G/S_R, the different

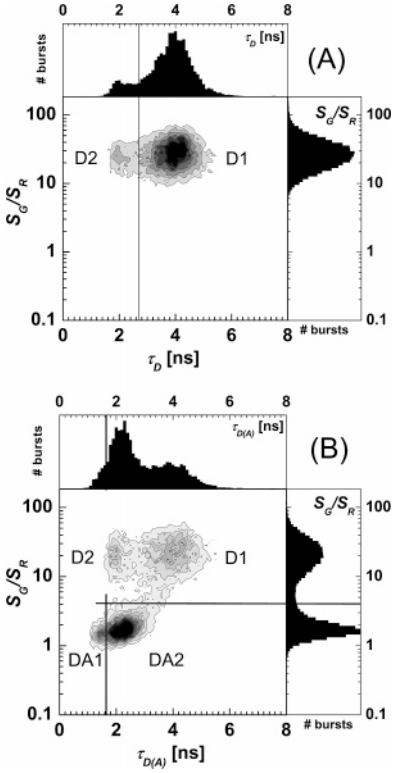

Figure 3. S_G/S_R vs $\tau_{D(A)}$ based selection of DNA molecules. (A) Donor-only DNA construct. The selection rule at $\tau_{D(A)} = 2.7$ ns divides the data into two regions corresponding to two different quantum yields for this dye. Only molecules with $\tau_{D(A)} > 2.7$ ns are further analyzed. (*B*) DA-13 DNA construct. (D and A are 13 bp apart.) Two selection criteria were used for this sample ($\tau_{D(A)} > 1.8$ ns and $S_G/S_R < 4$) due to additional peaks caused by bleaching and incomplete labeling.

lifetimes lead to different brightnesses and consequently to different $P(N)$ distributions. Therefore, only molecules from D1 were selected for time window analysis, as indicated by the vertical line at $\tau = 2.7$ ns in Figure 3A.

A histogram of the S_G/S_R signal after a time window analysis with a window size of 1 ms is shown in Figure 2B (gray shaded area). The best-fit PDA histogram occurs for $\langle F_G/F_R \rangle = \infty$, i.e., no red fluorescence (Figure 2B, black line). The excellent agreement between the theory and the experiment validates our assumptions regarding the homogeneity of the system, and even in the limit of $E = 0$ the PDA method is valid. In particular, the lack of broadening indicates that there is no spectral diffusion or brightness variation within the selected species, confirming that the dye linked to DNA is in a homogeneous environment. The short-lifetime species (D2) was similarly analyzed and also resulted in excellent agreement between the measurements and the PDA distribution, with the optimal $\langle F_G/F_R \rangle$ again being infinity (data not shown).

4.4. DNA FRET Pair. Having verified that a single dye has a homogeneous behavior on the time scale of our measurements, the actual FRET DA-13 DNA was investigated. As with the donor-only sample, the existence of two FRET species as shown in Figure 3B required a selection procedure that ensured that only species DA2 was analyzed ($\tau > 1.8$ ns, $S_G/S_R < 4$). A subsequent time window analysis produced an S_G/S_R histogram with a broad peak and a long tail, as shown in Figures 4A and 4B (gray shaded areas). An attempt to fit the histogram with a single $\langle F_G/F_R \rangle$ value resulted in the dotted line histogram in Figure 4A. It is obvious that in this case the PDA method fails to describe the data correctly, indicated by a χ^2 value of 124.

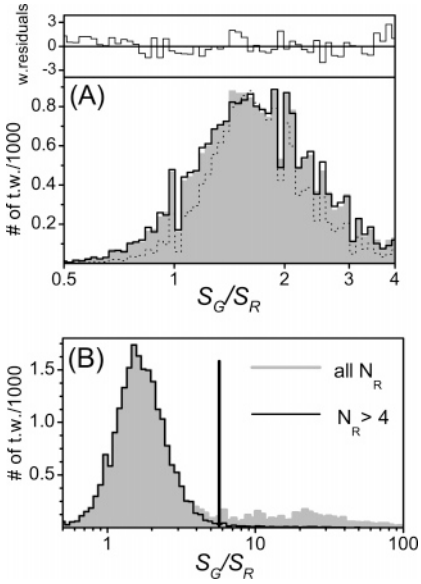

Figure 4. Histograms of the number of time windows with particular S_G/S_R values calculated from the DA-13 DNA data. (A) S_G/S_R histogram calculated from the data (gray area) and predicted from the PDA method for both a fixed fluorescence ratio ($\langle F_G/F_R \rangle = 1.61$, dotted line) and a model Gaussian distance distribution with a center of $\overline{\langle F_G/F_R \rangle} = 1.58$ and $\sigma_{ratio} = 0.07$ (solid line), which corresponds to $\bar{R}_{DA} = 53.9$ Å and $\sigma_R = 2.3$ Å. The data were fit to a Gaussian distribution of distances in the range from 0.5 to 4.0. $\langle B_G \rangle = 3.83$ counts, $\langle B_R \rangle = 1.15$ counts, $\alpha = 0.01$, $\Phi_{FA} = 0.32$, $\Phi_{FD} = 0.80$, $g_R/g_G = 2.2$, and $\chi^2 = 1.03$. $N = 20-444$. A threshold of 20 was chosen to ensure that a $\tau_{D(A)}$ value could be calculated for each time window and to avoid photobleaching events in DA-13 DNA. (B) Remaining effects of bleaching and blinking in S_G/S_R. The gray histogram shows the S_G/S_R signal as analyzed in Figure 4A but including the long tail at $S_G/S_R > 4$ (vertical line). The black line histogram shows the same data after removing time windows with <4 red photons, i.e., time windows with only background red photons. The histogram tail corresponding to $S_G/S_R > 4$ is largely removed, whereas the active species peak is not significantly affected, suggesting that the tail is due to time windows with an inactive acceptor.

There are many possible reasons that may cause a broadening of the S_G/S_R distributions beyond the shot-noise limit. Several will be discussed in detail in section 5.3, but the analysis will be continued here assuming that the broadening is due to fluctuations in the DA distances. This assumption is not unreasonable when the long and flexible linkages of Alexa488 and Cy 5 are considered (12 and 13 atoms, respectively)[21] and is further supported by recent reports also using flexible linked reporter molecules.[22]

The DA distance, R_{DA}, influences the FRET efficiency according to $E = R_0^6/(R_{DA}^6 + R_0^6)$, which in turn influences ϵ through eq 8. Therefore, eq 5 must be extended to include a distribution in ϵ as a function of R_{DA} as shown in eq 9

$$P\left(\frac{S_G}{S_R}\right)_i = \int P(\epsilon(R_{DA})) \sum_{\substack{\text{all } N,F_{RT},B_G,B_R \\ \text{which yield } (S_G/S_R)_i}} P(N)P_\epsilon(F_{RT}|N - B_G - B_R)P_{\langle B_G \rangle}(B_G)P_{\langle B_R \rangle}(B_R)\, d\epsilon \quad (9)$$

An expression for $\epsilon(R_{DA})$ can be derived from eq 8 by expressing E in terms of R_0 and R_{DA}. If the distribution for R_{DA} is known, then a distribution for $\epsilon(R_{DA})$ can be derived that can be used to evaluate eq 9. Assuming a Gaussian distribution of distances[7] described by an average distance $\bar{R}_{DA}$ and standard deviation in the distance of σ_R, $P(\epsilon(R_{DA}))$ becomes[21]

$$P(\epsilon(R_{DA})) = \frac{R_0}{6\sqrt{2\pi}\sigma_R}\left(\frac{\Phi_{FA}g_R}{\Phi_{FD}g_G}\right)^{1/6}\frac{1}{(1-\epsilon)^2}\left(\frac{1}{1-\epsilon}-(1+\alpha)\right)^{-7/6}\times \exp\left\{-\frac{1}{2\sigma_R{}^2}\left[R_0\left(\frac{\Phi_{FA}g_R}{\Phi_{FD}g_G}\right)^{1/6}\left(\frac{1}{1-\epsilon}-(1+\alpha)\right)^{-1/6}-\bar{R}_{DA}\right]^2\right\} \quad (10)$$

Through the use of eqs 9 and 10, the PDA distribution was fit to the data by varying $\bar{R}_{DA}$ and σ_R. The best fit, shown as the solid line in Figure 4A, occurred at values of $\bar{R}_{DA} = 53.9$ Å and $\sigma_R = 2.3$ Å, with no systematic deviation in the weighted residuals (Figure 4A, top). The histogram was fit only in the range from $0.5 < S_G/S_R < 4$ because bleaching and blinking of the acceptor dye in some time windows resulted in additional signal at higher ratios (see below).

5. Discussion

5.1. Histogram Features. The probability spikes and voids observed in Figure 1 lead to histogram distributions that are sensitive to the choice of bin width and position and to histogram distributions that are rough. Figure 1 shows two histograms calculated using 49 bins (gray area) and 50 bins (solid line). A 1 bin change shifts the positions of the maximum and two satellite peaks. As the maximum count N decreases, the dependence of the histogram shape on the bin parameters increases. Additionally, the histogram roughness increases, making it difficult to assign a characteristic shape to the peaks. These problems are typically addressed in single-molecule experiments by the use of larger time windows and minimum threshold criteria that serve to smooth the histograms[15] but simultaneously lower time resolution and hide real information.

The relative sizes of the spikes proved to be very sensitive to $\langle F_G/F_R\rangle$. For example, $P(1)/P(2)$ changes by an order of magnitude, from 20 to 2, as the expected fluorescence ratio $\langle F_G/F_R\rangle$ changes from 0.7 to 1.3.[21] The model is therefore very sensitive to changes in $\langle F_G/F_R\rangle$ within this range. Considering all of the spikes together over the entire histogram provides a molecular "bar code" that provides a sensitive determination of $\langle F_G/F_R\rangle$ over a broad range.

5.2. Shot-Noise-Limited Fluorescence Distributions. A key result of this work as shown in Figure 2A is the ability of the PDA method to fit FRET fluorescence ratios to uncorrected data unambiguously and precisely in a way that is independent of the threshold and the number of bins. The value determined for $\langle F_G/F_R\rangle$ was largely insensitive to changes in either of these parameters, never varying by more than 1% as either the number of bins or minimum number of photons were changed.[21] The insensitivity of $\langle F_G/F_R\rangle$ to the threshold level means that the threshold count criterion can be significantly lowered and the size of the time windows decreased.

The χ^2 was very sensitive to the value of $\langle F_G/F_R\rangle$. The minimum χ^2 value was 1.3 at a ratio of 4.02. The error of the fit was estimated by determining at what $\langle F_G/F_R\rangle$ value did χ^2 increase to 2.3 or one higher than the minimum. This criterion was satisfied at ratio values of 3.95 and 4.09, indicating an error of a 1.8% in determining the fluorescence ratio.

5.3. Signal Broadening. Broadening of the S_G/S_R distribution occurs because the $P(N)$ and/or the P_ϵ distributions in eq 5 vary during the measurements, causing brightness and/or apparent efficiency fluctuations. There are several mechanisms that can result in such fluctuations. A few of the possible mechanisms are discussed below, but others probably exist. First, it is possible that the dyes exist in more than one active state. Figure 3 demonstrates that Alexa488 has two species with different lifetimes, and Cy5 is known to exhibit double-exponential decay behavior and to possess nonfluorescent intermediates that are capable of quenching the donor.[23,24] Second, the shape of a confocal detection volume is wavelength-dependent, so it is possible that the ratio g_G/g_R is position-dependent and changes as the molecule diffuses through the focus. A third possibility is that E changes due to a changing R_0, either due to spectral shifts in the dyes, changes in Φ_{FD}, or changes in the geometric orientation factor κ^2. A fourth mechanism is changes in E caused by a variation in R_{DA}, as already discussed in section 4.4. The evidence favors the latter explanation. Each of these possibilities are discussed below, but first the time scale on which variations must occur to cause signal broadening are discussed.

5.3.1. Time Scales for Dynamics. If a molecule undergoes dynamics at a rate faster than the photon count rate, then consecutive photons are uncorrelated with respect to which state produced them; i.e., the state for each photon is independent and randomly determined. In this case, there is a fixed probability, $P(i)$, that the molecule is in the ith state when a photon is emitted. If the FRET efficiency of the ith state is a constant E_i, then the probability of both being in the ith state and transferring energy is $P(i) \times E_i$. It follows that the expected probability of transferring energy is given by $\langle E\rangle = \sum_i P(i) \times E_i$; i.e., dynamics result in a constant $\langle E\rangle$, and in the limit of dynamics occurring much faster than photon counting, the signal histograms approach a single shot-noise-limited PDA distribution. It is therefore sufficient to show that dynamics are fast compared to count rates to exclude them as a source of broadening.

Dynamics may also occur on a time scale approaching the size of the time windows used in the analysis. In this case, the likelihood that entire time windows will pass without a dynamic event occurring is significant and will result in a distinct shot-noise-limited peak for each species with a long duration. Therefore, slow dynamics result in multiple shot-noise-limited peaks and are easily recognized.

In these experiments, maximum count rates were typically 100 kHz, and a 1 ms time window analysis was used. Only dynamics that occurred within the time scale of 10−500 μs could result in broadening.

5.3.2. Multiple States of Alexa488 and Cy5. The two species of Alexa488 are clearly resolvable in the burstwise analysis in Figure 3, and a time window analysis of either peak produced a shot-noise-limited distribution. Furthermore, FCS measurements did not show any brightness fluctuations in the 10−500 μs range. Therefore, fluctuations in Alexa488 are too slow to cause broadening and are excluded.

Cy5 has been extensively studied for use as an acceptor dye in DNA experiments.[18,25] In these experiments, Cy5 was shown to undergo intersystem crossing to a triplet state and triplet deactivation with rates of $k_{ISC} = 0.5 \times 10^6$ s^{-1} and $k_T = 0.2 \times 10^6$ s^{-1}, respectively. Cy5 also displays photon-dependent isomerization between a strongly fluorescent trans state and a weakly fluorescent cis state. Under the excitation intensities used here, the isomerization rate is $k_{ISO} = 0.16 \times 10^6$ s^{-1}. An FCS analysis (Figure 5) of the red signal did not show any brightness fluctuations in the 10−500 μs range. Therefore dynamics of the dyes are ruled out as mechanisms that cause broadening.

5.3.3. Inhomogeneous g_G/g_R. The focus volume can be ideally described by a wavelength-dependent three-dimensional Gaussian function.[27] Through the use of two different color ranges, it is conceivable that the observation foci have different sizes,

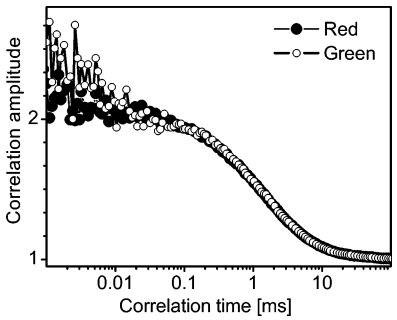

Figure 5. Selective FCS studies[26] of DA-13 DNA molecule signals. Open circles correspond to the donor signal, and solid circles correspond to the acceptor signal. Fits of the FCS curves determined the donor and acceptor diffusion times to be 1.23 and 1.27 ms, respectively, indicating similar detection volumes for the two dyes. The triplet time of Alexa488 and the isomerization time for Cy5 were determined to be 0.9 and 5.0 μs, respectively. Neither dye shows dynamics in the time scale 10−500 μs.

resulting in a position-dependent g_G/g_R. This artifact was avoided by not focusing the optics to a diffraction-limited spot size where wavelength effects become significant and by illuminating only molecules in a portion of the observation volume near the center, where a Gaussian volume shows the lowest spatial variation ($\omega_{0E} < \omega_{0O}$). Thus g_G/g_R remains constant within our ability to measure, which is confirmed by both the FCS measurements in Figure 5 indicating no measurable differences in the detection volumes for green and red and the success of predicting shot-noise-limited single-dye and donor-only distributions.

5.3.4. Förster Radius. The Förster radius is calculated as $R_0 = 9870\ [\Phi_{FD} J(\lambda) \kappa^2\ n^{-4}]^{1/6}$, where n is the index of refraction of the medium, κ^2 is a geometric orientation factor, and $J(\lambda)$ is the overlap integral between the donor emission and the acceptor adsorption spectra. Broadening due to changes in Φ_{FD} have already been excluded. Changes in κ^2 could be caused by slow rotational motions of either dye. Previous studies have shown that the mean rotational correlation times of Alexa488 and Cy5 attached to DNA are 0.6 and 2.3 ns, respectively.[18] These values are too short to cause broadening in these measurements. Finally, a spectral shift for either dye would result in a time-varying $J(\lambda)$. A spectral shift would also lead to a change in the detection efficiency, which would be detectable as a fluctuation in intensity. No fluctuations in the 10−500 μs time range were detectable via an FCS analysis (Figure 5) for either the green or the red signal. Additionally, the donor-only measurements specifically verified the lack of spectral shifts in Alexa488. Therefore, spectral shifts, and changes in R_0 altogether, are excluded as sources for the observed broadening.

5.3.5. Cy5 Bleaching. As explained in section 4.4, only molecule bursts corresponding to peak DA2 in Figure 3B were selected for time window analysis. After this analysis, time windows appeared with high S_G/S_R values (Figure 6). Dividing a burst into time windows lowers the number of photons used to calculate fluorescence parameters. In combination with the random signal variations within a burst, broader histograms are expected. However, despite having enough windows for a good statistical sampling, Figure 6 shows a more extreme behavior. These molecules have distinct populations of time windows with $S_G/S_R \approx 30$ and $\tau_{D(A)}$ values ranging from 2 to 4 ns. The heterogeneous $\tau_{D(A)}$ results in brightness fluctuations that make fitting these time windows to a donor-only PDA distribution impossible. Figure 7 shows a time trace of a single burst using a sliding window of 100 μs. This molecule undergoes single-step acceptor bleaching (event indicated by a vertical line), resulting in a synchronous rise in green intensity and lifetime.

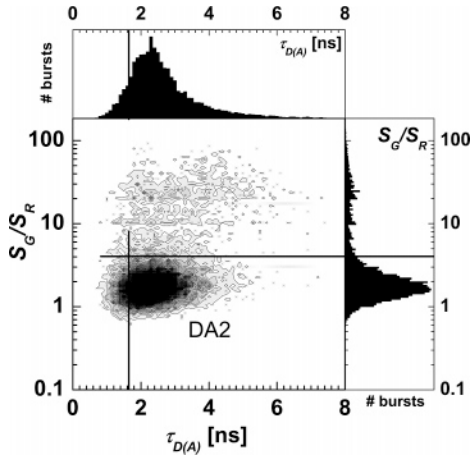

Figure 6. S_G/S_R vs $\tau_{D(A)}$ diagram of DA-13 DNA signal after time window analysis of species DA2 from Figure 3B. DA2 remains visible, but a broad, weak signal at $S_G/S_R > 4$ appears with $\tau_{D(A)}$ distributed from 2 to 4 ns. The signal is likely due to weakly or nonfluorescent Cy5 molecules, resulting in the high signal ratios. The broad distribution in $\tau_{D(A)}$ indicates a mixture of bleached, inactive Cy5 and dark Cy5 states that are still capable of quenching the donor. Multiple dark states may exist.

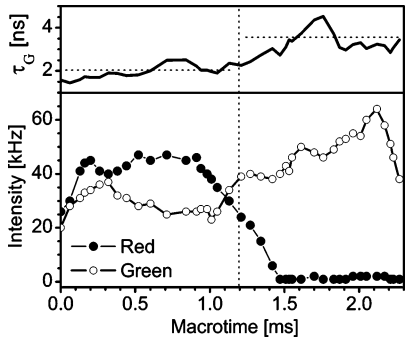

Figure 7. Fluorescence signal within a burst. The intensity of the green and red intensities below (solid circles and open circles, respectively) and the green lifetime above. Cy5 undergoes single-step bleaching, with a simultaneous rise in green intensity and a fall in red intensity, together with a corresponding rise in green lifetime. To generate enough points for a visual presentation, the data was calculated from overlapping 1 ms time windows (100 μs shift), which results in the single-step transition (vertical dotted line) being significantly smoothed. Horizontal dotted lines indicate the average green lifetimes before and after the transition.

After acceptor bleaching, molecules exhibit an unquenched, donor-only-like signal. In addition, Cy5 can enter dark states during a burst and then recover. Dark states have been observed in Cy5[23,24] and Cy5 attached to DNA[23,28] as intermediates to a bleached state. These studies suggested that there are at least two intermediate states still capable of quenching a donor. A mixing of dark states, fluorescence, and bleached states would explain the $\tau_{D(A)}$ distribution in Figure 6.

One feature common to the intermediates and the bleached state is that they produce a red signal that is close to the background. A look at the red intensity distribution, $P(N_R)$, in Figure 8 (gray histogram) reveals two peaks, corresponding to the fluorescent and nonfluorescent states. An overlay of the $P(N_R)$ distribution from the donor-only experiment (black line) suggests a selection criterion of $N_R > 4$ will exclude most of the dark Cy5 time windows from the analysis. Furthermore, the existing criterion of $N \geq 20$ for all of the analyses makes it unlikely that a fluorescence-active species will produce four or fewer red photons, so the FRET time windows should not be affected. Figure 4B presents the data as analyzed in Figure 4A

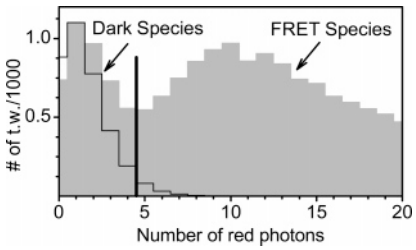

Figure 8. Bleaching and blinking in red intensity distributions. The histograms count the number of time windows with a given number of red photons. The gray histogram shows the intensity distribution of the DA-13 DNA FRET data in Figure 4. Two peaks are seen: a low FRET or dark Cy5 species at $N_R < 5$, which most likely contains bleached and dark Cy5 molecules, and a FRET Cy5 active species. The black line histogram is the intensity distribution of the red signal from the donor-only sample shown in Figure 2B, shown for comparison. The slight difference in the average intensities of the donor-only distribution and dark Cy5 species of the DA-13 DNA (<1 photon/time window) is likely due to a minimal amount of fluorescence from the dark species.

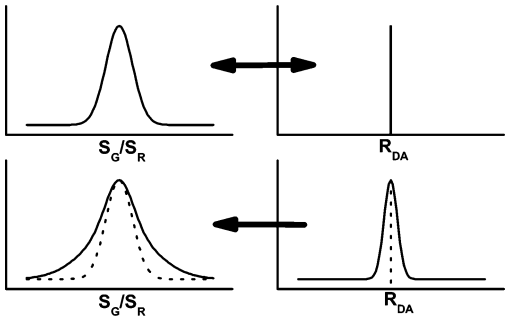

Figure 9. Schematic illustration of (above) a shot-noise-limited distribution resolved into a single originating value and visa versa, whereas (below) a broader distribution must originate from a distribution of values.

(gray histogram) and the same data analyzed with the additional $N_R > 4$ criterion. The signal at $S_G/S_R > 4$ has been almost completely removed, while the FRET peak remains virtually unchanged.

On the basis of the PDA histogram in Figure 2B, it is possible to estimate that ~6.5% of a donor-only signal has an $S_G/S_R \leq 4$, which when applied to Figure 4B suggests that 282 time windows in the FRET peak are actually from the donor-only population. Alternatively, Figure 8 indicates that ~10% of the donor-only time windows (329) survive the N_R threshold, without commenting on the S_G/S_R value. In practice, only those windows that survive both of these criteria will appear in the filtered histogram of Figure 4B (black line). The total difference between the shot-noise-limited distribution and the data in Figure 4A is 6715 time windows, indicating that the number of possible bleached and dark bursts is not large enough to explain the observed broadening.

6. Conclusions

The PDA method predicts the shot-noise-limited distribution of a two-color FRET signal, thereby describing the minimum width that a FRET signal distribution must have given existing background, crosstalk, and efficiency. Conversely, as schematically presented in Figure 9, the PDA method can successfully extract the originating value behind shot-noise-limited FRET signal distributions and determine the underlying fluorescence signal ratio with a precision of better than 2%. Under optimal conditions, this precision translates into a precision in the distance measurements better than 1% of the Förster radius. FRET distributions that are not shot-noise-limited are easily identified. For these distributions the PDA method can be used to test the validity of models used to explain the additional broadening. Here, a 5 Å distribution broadening due to the mobility of the dyes on flexible linkers is easily revealed. The surprisingly slow linker movements identified here can be rationalized by the existence of a rugged potential surface defined by the presence of the DNA, which hinders the free movement of the dyes.

Information describing the distribution of distances in molecules is valuable in determining protein intermediates and exploring partially folded states and refolding mechanisms. Furthermore, the success of the model even for low photon counts allows both smaller time windows providing higher time resolution and lower photon thresholds, which increases number of bursts that can be used in an analysis.

Especially significant in this work is that eqs 9 and 10 fit a distribution of distances to uncorrected experimental data. The standard practice of subtracting background and crosstalk correction factors from the data ultimately leads to a large number of negative values that confuse the interpretation of the data. Here, the background and crosstalk signals are instead added to the PDA distributions, an approach that allows a direct comparison between the model and the data.

Acknowledgment. We thank Jerker Widengren for his helpful discussions, Stanislav Kalinin for his modeling suggestions, and Alessandro Valeri and Enno Schweinberger for their assistance. Funding for this project was provided by the VW Stiftung I/78 837 and DFG SPP 1170.

Supporting Information Available: Peak ratio sensitivity to $\langle F_G/F_R \rangle$ value, PDA features, goodness of fit dependence on number of bins and threshold, apparent fluorescence efficiency probability density distribution, and background histogram correcting procedure. This material is available free of charge via the Internet at http://pubs.acs.org.

References and Notes

(1) Haas, E. *ChemPhysChem* **2005**, *6*, 858−870.
(2) Dahan, M.; Deniz, A. A.; Ha, T. J.; Chemla, D. S.; Schultz, P. G.; Weiss, S. *Chem. Phys.* **1999**, *247*, 85−106.
(3) Kapanidis, A. N.; Laurence, T. A.; Lee, N. K.; Margeat, E.; Kong, X. X.; Weiss, S. *Acc. Chem. Res.* **2005**, *38*, 523−533.
(4) Lu, H. *Acc. Chem. Res.* **2005**, *38*, 557−565.
(5) Ha, T.; Enderle, T.; Ogletree, D. F.; Chemla, D. S.; Selvin, P. R.; Weiss, S. *Proc. Natl. Acad. Sci. U.S.A.* **1996**, *93*, 6264−6268.
(6) Eggeling, C.; Fries, J. R.; Brand, L.; Günther, R.; Seidel, C. A. M. *Proc. Natl. Acad. Sci. U.S.A.* **1998**, *95*, 1556−1561.
(7) van der Meer, B. W.; Cooker, G.; Chen, S. Y. *Resonance Energy Transfer: Theory and Data*; VCH Publishers: New York, 1994.
(8) Diez, M.; Zimmermann, B.; Börsch, M.; König, M.; Schweinberger, E.; Steigmiller, S.; Reuter, R.; Felekyan, S.; Kudryavtsev, V.; Seidel, C. A. M.; Gräber, P. *Nat. Struct. Mol. Biol.* **2004**, *11*, 135−141.
(9) Margittai, M.; Widengren, J.; Schweinberger, E.; Schröder, G. F.; Felekyan, S.; Haustein, E.; König, M.; Fasshauer, D.; Grubmüller, H.; Jahn, R.; Seidel, C. A. M. *Proc. Natl. Acad. Sci. U.S.A.* **2003**, *100*, 15516−15521.
(10) Schuler, B.; Lipman, E. A.; Eaton, W. A. *Nature* **2002**, *419*, 743−747.
(11) Schuler, B.; Lipman, E. A.; Steinbach, P. J.; Kumke, M.; Eaton, W. A. *Proc. Natl. Acad. Sci. U.S.A.* **2005**, *102*, 2754−2759.
(12) Xie, Z.; Srividya, N.; Sosnick, T. R.; Pan, T.; Scherer, N. F. *Proc. Natl. Acad. Sci. U.S.A.* **2004**, *101*, 534−539.
(13) Deniz, A. A.; Dahan, M.; Grunwell, J. R.; Ha, T. J.; Faulhaber, A. E.; Chemla, D. S.; Weiss, S.; Schultz, P. G. *Proc. Natl. Acad. Sci. U.S.A.* **1999**, *96*, 3670−3675.
(14) Gopich, I.; Szabo, A. *J. Chem. Phys.* **2005**, 014707.
(15) Watkins, L. P.; Yang, H. *Biophys. J.* **2004**, *86*, 4015−4029.
(16) Fries, J. R.; Brand, L.; Eggeling, C.; Köllner, M.; Seidel, C. A. M. *J. Phys. Chem. A* **1998**, *102*, 6601−6613.

(17) Rothwell, P. J.; Berger, S.; Kensch, O.; Felekyan, S.; Antonik, M.; Wöhrl, B. M.; Restle, T.; Goody, R. S.; Seidel, C. A. M. *Proc. Natl. Acad. Sci. U.S.A.* **2003**, *100*, 1655−1660.

(18) Widengren, J.; Schweinberger, E.; Berger, S.; Seidel, C. A. M. *J. Phys. Chem. A* **2001**, *105*, 6851−6866.

(19) Eggeling, C.; Berger, S.; Brand, L.; Fries, J. R.; Schaffer, J.; Volkmer, A.; Seidel, C. A. M. *J. Biotechnol.* **2001**, *86*, 163−180.

(20) Eggeling, C.; Widengren, J.; Brand, L.; Schaffer, J.; Felekyan, S.; Seidel, C. A. M. *J. Phys. Chem. A* **2006**, *110*(9), 2979−2995.

(21) See the Supporting Information to this paper.

(22) Hilger, D.; Jung, H.; Padan, E.; Wegener, C.; Vogel, K.-J.; Steinhoff, H.-J.; Jeschke, G. *Biophys. J.* **2005**, *89*, 1328−1338.

(23) Heilemann, M.; Margeat, E.; Kasper, R.; Sauer, M.; Tinnefeld, P. *J. Am. Chem. Soc.* **2005**, *127*, 3801−3806.

(24) Bates, M.; Blosser, T. R.; Zhuang, X. *Phys. Rev. Lett.* **2005**, *94*, 108101.

(25) Widengren, J.; Schwille, P. *J. Phys. Chem. A* **2000**, *104*, 6416−6428.

(26) Böhmer, M.; Wahl, M.; Rahn, H. J.; Erdmann, R.; Enderlein, J. *Chem. Phys. Lett.* **2002**, *353*, 439−445.

(27) Rigler, R.; Mets, Ü.; Widengren, J.; Kask, P. *Eur. Biophys. J.* **1993**, *22*, 169−175.

(28) Ha, T.; Xu, J. *Phys. Rev. Lett.* **2003**, *90*, 223002.